CELL BIOLOGY

A persulfidation-based mechanism controls aquaporin-8 conductance

Stefano Bestetti,[1]* Iria Medraño-Fernandez,[1]*† Mauro Galli,[1] Michela Ghitti,[2] Gerd P. Bienert,[3] Giovanna Musco,[2] Andrea Orsi,[1] Anna Rubartelli,[4] Roberto Sitia[1]†

Upon engagement of tyrosine kinase receptors, nicotinamide adenine dinucleotide phosphate (NADPH)–oxidases release H_2O_2 in the extracellular space. We reported previously that aquaporin-8 (AQP8) transports H_2O_2 across the plasma membrane and is reversibly gated during cell stress, modulating signal strength and duration. We show that AQP8 gating is mediated by persulfidation of cysteine 53 (C53). Treatment with H_2S is sufficient to block H_2O_2 entry in unstressed cells. Silencing cystathionine β-synthase (CBS) prevents closure, suggesting that this enzyme is the main source of H_2S. Molecular modeling indicates that C53 persulfidation displaces a nearby histidine located in the narrowest part of the channel. We propose that H_2O_2 molecules transported through AQP8 sulfenylate C53, making it susceptible to H_2S produced by CBS. This mechanism tunes H_2O_2 transport and may control signaling and limit oxidative stress.

INTRODUCTION

Cysteine sulfurs can undergo many redox-dependent modifications (-SS-, -SOH, $-SO_2H$, $-SO_3H$, -SNO, and -SSH) providing versatile switches for tuning protein activity and stability and hence influencing a wide variety of cellular pathways. Key second messengers in redox regulation are hydrogen peroxide (H_2O_2) (*1*) and hydrogen sulfide (H_2S) (*2*). Upon activation of tyrosine kinase receptors, H_2O_2 is produced by NAPDH-oxidases (NOX) in the outer leaflet of the plasma membrane. To reach its cytosolic targets, H_2O_2 exploits proteinaceous channels like aquaporin-3 (AQP3), AQP8, and AQP9 (*3*–*6*). In mammals, H_2S biosynthesis depends mainly on two pyridoxal phosphate-dependent enzymes of the transsulfuration pathway, cystathionine β-synthase (CBS) and cystathionine γ-lyase (CSE) (*7*). A third source of H_2S is 3-mercaptopyruvate sulfur transferase, an enzyme that predominantly resides in mitochondria (*8*). H_2S reacts preferentially, if not exclusively, with oxidized cysteines (-SOH or -SS-), leading to the formation of R-S-SH moieties in target proteins (*9*, *10*). This reversible process is called S-sulfhydration or persulfidation and is pivotal in redox homeostasis (*11*, *12*). H_2S limits oxidative stress and prevents cell death (*12*, *13*), while its deficiency promotes cellular aging (*14*), suggesting that persulfidation may protect proteins from irreversible oxidation (*15*). However, diverse effects reported in the literature hint that H_2S signals are integrated with other circuits (*16*, *17*), allowing adaptation to different cellular needs (*8*).

As a gaseous compound, H_2S is thought to cross cell membranes without the need of dedicated transport mechanisms (*18*, *19*). This is not the case for H_2O_2: Peroxiporins provide an additional level to control the intensity of tyrosine kinase signaling [reviewed by Bienert *et al.* (*20*)]. We have recently shown that AQP8 is reversibly gated by redox-dependent modifications of cysteine 53 (C53) in cells undergoing diverse stresses (*21*). Considering that most stresses entail production of reactive oxygen species (ROS) (*22*, *23*) and H_2S (*24*, *25*), we investigated whether a two-step sulfenylation-persulfidation process could be the mechanism that reversibly gates AQP8.

[1]Protein Transport and Secretion Unit, Division of Genetics and Cell Biology, Istituto di Ricovero e Cura a Carattere Scientifico (IRCCS) Ospedale San Raffaele, Università Vita-Salute San Raffaele, 20132 Milan, Italy. [2]Biomolecular Nuclear Magnetic Resonance (NMR) Unit, Division of Genetics and Cell Biology, IRCCS Ospedale San Raffaele, Università Vita-Salute San Raffaele, 20132 Milan, Italy. [3]Metalloid Transport Group, Leibniz Institute of Plant Genetics and Crop Plant Research, 06466 Gatersleben, Germany. [4]Cell Biology Unit, IRCCS Azienda Ospedaliera Universitaria (AOU) San Martino-IST, 16132 Genoa, Italy.
*These authors contributed equally to this work.
†Corresponding author. Email: sitia.roberto@hsr.it (R.S.); medranofernandez.iria@hsr.it (I.M.-F.)

RESULTS

H_2S inhibits H_2O_2 cell permeability

When HeLa cells stably expressing a cytosolic HyPer probe (*26*) are exposed to H_2O_2, a strong increase in the probe fluorescence is detected (Fig. 1A, red trace). Addition of the membrane-permeant reducing agent dithiothreitol (DTT) causes an initial, rapid decrease in the signal. The slower decay that follows likely reflects the combined action of HyPer reduction by DTT and its oxidation by H_2O_2 still entering into cells. Accordingly, quenching extracellular H_2O_2 by adding a catalase before DTT causes a drastic decrease in HyPer activation (Fig. 1B, red trace).

We then used sodium hydrogen sulfide (NaSH) as an exogenous source of H_2S. NaSH rapidly dissociates into Na^+ and HS^-, about one-third of which form H_2S at physiological pH (*27*). Addition of NaSH blocked H_2O_2 import (Fig. 1A, blue trace), mimicking the inhibition we previously described under stress conditions (*21*). The blockade was time- and concentration-dependent (fig. S1, A and B) and, as observed for stress, reversible (fig. S1C).

Unexpectedly, in H_2S-treated cells, DTT caused a transient oxidation of HyPer (Fig. 1A, blue trace). The presence of catalase prevented this DTT-induced oxidative spike (Fig. 1B, blue trace). Thus, H_2S did not directly inhibit HyPer but rather caused modifications of H_2O_2 transporters that can be reversed by DTT, as we showed before for stress conditions (*21*). To confirm this hypothesis, we used sodium 2-mercaptoethanesulphonate (MESNA), a reductant that, being unable to cross the plasma membrane, cannot directly act on HyPer. Consistent with channel reopening due to removal of a redox modification, treatment with MESNA allowed entry of exogenous H_2O_2 (Fig. 1C, blue trace) more efficiently than DTT because it could not reduce HyPer. MESNA increased HyPer activation also in nontreated cells (Fig. 1C, red trace), suggesting that H_2O_2 channels undergo partial oxidative inhibition also at steady state.

In our cellular model, AQP8 was the target of the stress-induced gating, which hits C53 (*4*, *21*). If this were also true for H_2S-induced inhibition, then treatment with NaSH should not hamper H_2O_2 import in cells expressing the AQP8 C53S mutant, which was insensitive to the stress-induced blockade (*21*). As expected, HeLa transfectants expressing

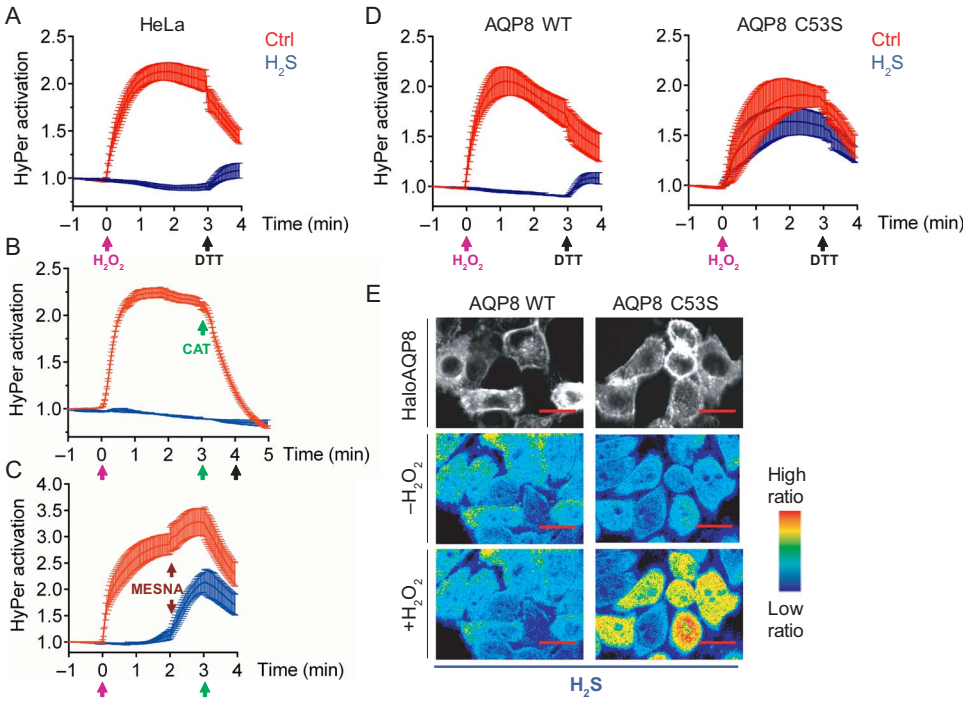

Fig. 1. H_2S blocks AQP8-dependent H_2O_2 transport. (**A** to **C**) The kinetics of HyPerCyto activation in HeLa cells upon addition of 50 μM H_2O_2 and with or without a pretreatment with H_2S (blue and red traces, respectively). Colored arrows indicate the time at which indicated compounds were added to cells (5 mM DTT, black; 5000 U/ml of catalase, green; and 10 mM MESNA, brown). (**D**) Time course of HyPer activation in HeLa cells expressing either HaloAQP8 WT (left graph) or the C53S mutant (right graph) upon addition of 50 μM H_2O_2 and treated with or without H_2S. Only cells expressing the transgene were analyzed [see (E)]. In all cases (A to D), data are shown as mean fold changes of the 488/405-nm ratio measured by confocal laser scanning, plotted against time. Mean of ≥3 experiments are shown ± SEM. Ctrl, control. (**E**) Frames extracted from time course analyses of H_2O_2 import on cells expressing WT or C53S HaloAQP8 treated with H_2S. Cells expressing the transgene are stained by fluorescent Halo ligands (upper frames). The 488/405-nm ratio intensity, represented in pseudocolor, reflects the activation of HyPerCyto upon addition of 50 μM H_2O_2 (lower frames). Note that the sensor is activated only in C53S-expressing cells. Scale bars, 50 μm.

wild-type AQP8 (AQP8 WT) could not import H_2O_2 upon treatment with H_2S, and DTT induced a transient spike (Fig. 1D, left panel, blue trace), as noted before for nontransfected cells. By contrast, C53S transfectants were resistant to inhibition (Fig. 1D, right panel, blue trace), and DTT addition caused HyPer reduction irrespective from H_2S treatment (Fig. 1D, black arrow). Single-cell analyses confirmed the role of C53 (Fig. 1E and movies S1 and S2). Only cells expressing the mutant, identified by staining with Halo ligands (Fig. 1E, upper panel), responded to H_2O_2 after H_2S treatment. Neither nontransfected cells nor WT transfectants were able to import H_2O_2. Together, these data show that C53 is the main target of H_2S in AQP8.

CBS is required for stress-dependent AQP8 inhibition

CBS is a pivotal enzyme in the mammalian transsulfuration pathway (*28*). It catalyzes either the condensation of serine and homocysteine or cysteine desulfuration, yielding H_2S in both processes. Considering that CBS activity is redox-regulated and increased during stress (*29*), we explored the possibility that this enzyme constitutes the endogenous source of H_2S controlling H_2O_2 transport. Therefore, we efficiently silenced its expression (fig. S2A) and monitored H_2O_2 transport before or after heat stress. CBS down-regulation was sufficient to prevent stress-induced AQP8 gating (Fig. 2A, compare gray and light blue traces). Addition of exogenous H_2S blocked transport in CBS-silenced cells (Fig. 2A, green trace), excluding off-target effects of our silencing protocol. To further confirm the involvement of CBS on the mechanism closure, we heat-shocked HeLa cells in the presence of tangeretin, a

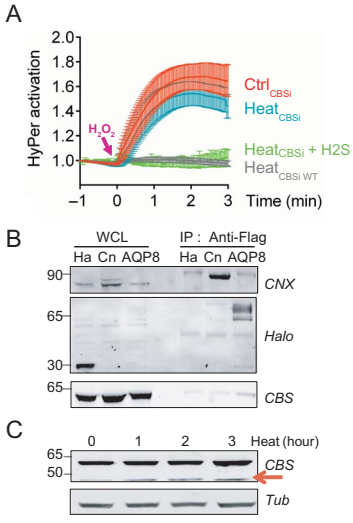

Fig. 2. CBS produces H_2S for AQP8 gating in heat-stressed cells. (**A**) H_2O_2 transport was analyzed as in Fig. 1 in HeLa cells expressing low (CBSi) or normal (CBS WT) levels of CBS. H_2O_2 entry into CBSi HeLa cells was no longer inhibited by heat stress (light blue trace), but treatment with H_2S restored inhibition (green trace). Mean of ≥3 experiments ± SEM. (**B**) Lysates from HeLa transfectants expressing a Flag-tagged HaloAQP8myc (AQP8), calnexin-Flag (Cn), or Halo (Ha) were immunoprecipitated with anti-Flag beads and immunoblotted with the indicated antibodies. WCL, whole cell lysate; IP, immunoprecipitation. (**C**) Aliquots from lysates of HeLa cells kept at 42°C for increasing times were blotted with the indicated antibodies. Note the appearance of a cleaved CBS form after heat shock.

specific CBS inhibitor (*30*), and we measured cell the capacity to import exogenous H_2O_2. As shown in fig. S2B, pharmacological inhibition of CBS also prevented aquaporin gating. In support of a role of CBS in modulating peroxiporin activity, the enzyme was in part co-immunoprecipitated with overexpressed AQP8 (Fig. 2B and fig. S2C). Moreover, heat stress caused the time-dependent appearance of a proteolytically cleaved form of CBS (Fig. 2C and fig. S2D), a process thought to be linked to redox-mediated enzyme activation (*31*).

AQP8 is gated by persulfidation of C53

The biotin-based biochemical methods used to detect sulfenylation or persulfidation (*9*, *32*–*35*) have failed so far to label C53, probably due to its poor accessibility within the AQP8 pore. To bypass this obstacle, we designed a strategy able to trace ^{35}S incorporation upon persulfide formation. The protocol exploits the notion that transsulfuration is the main route for removing sulfur-containing amino acids when in excess (*36*). Thus, we incubated cells with ^{35}S-methionine and ^{35}S-cysteine for 3 hours at 37° or 42°C in the presence of a protein synthesis inhibitor [cycloheximide (CHX)]. In these conditions (Fig. 3A), radioactive $H_2{}^{35}S$ should be generated leading to persulfidation of sensitive cysteines in proteins. Unlike radioactive amino acids inserted in the polypeptide backbone, the covalent R-S-^{35}SH groups can be removed by DTT. Therefore, even if some residual protein synthesis occurred during the 3-hour incubation, WT AQP8 should be more radioactive in cells exposed to stress than the C53S mutant, yielding stronger signals when gels are run under nonreducing conditions, but not after reduction of the immunoprecipitates. Accordingly, in nonreducing gels, the AQP8 bands were more intense in WT than in C53S after heat stress (Fig. 3B, top left panel, lanes +). Labeling the same immunoprecipitates with Halo ligands allowed quantification of the proteins loaded (Fig. 3B, lower panels). CHX did not completely inhibit the incorporation of ^{35}S-amino acids, yielding a background signal also in nonstressed cells, irrespective from the transgene expressed. Reduction of the samples before gel electrophoresis abolished the differences (Fig. 3B, top right panel, lanes +), indicating that the more intense signal in AQP8 WT reflected persulfidation of the C53 side chain by radioactive $H_2{}^{35}S$.

In our experiments, at least 30 min were required for H_2S to completely block H_2O_2 transport (fig. S1A), pointing to a nondirect inhibition mechanism. H_2S reacts poorly, if at all, with thiol or thiolate groups. Hence, persulfidation requires that the target cysteine residue be previously sulfenylated or disulfide bonded (*9*, *10*, *37*). C53 is located inside the AQP8 pore, far away from other cysteines, thus hindering intra- or intermolecular reactions with other thiols to form a disulfide (*21*). This

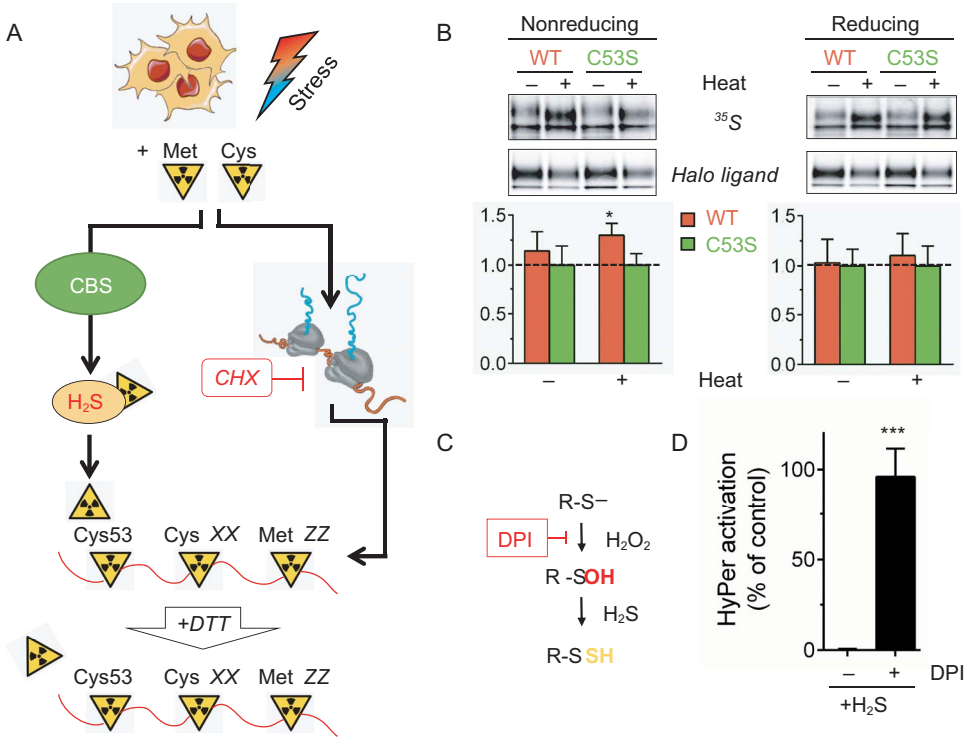

Fig. 3. Radioactive labeling of AQP8 persulfidation. (**A**) The scheme summarizes the protocol used to detect C53 persulfidation. Proteins can be radiolabeled by incorporating ^{35}S methionine and cysteine as building blocks during protein synthesis (right branch) or by reacting with $H_2{}^{35}S$ produced by the transsulfuration pathway (left branch). In the presence of protein synthesis inhibitors (0.5 mM CHX), the latter pathway should be favored, especially in conditions of stress that activate CBS. Unlike radioactive amino acids incorporated into proteins, –^{35}SH persulfide moieties are removed by a 200 mM DTT treatment, allowing discrimination from radioactive amino acids that are part of the polypeptide backbone. (**B**) Cells transfected with either WT or C53S HaloAQP8mycFlag were kept for 3 hours at 37° or 42°C (– or + heat, as indicated) in the presence of ^{35}S amino acids and CHX (0.5 mM). AQP8 was immunoprecipitated using anti-Flag beads, resolved under nonreducing or reducing conditions (left and right, respectively), and developed to detect the ^{35}S or Halo ligand signals to normalize protein synthesis and loading. The ratio between the ^{35}S and Halo ligand signals was calculated for each sample and values normalized to the values obtained with C53S (see Material and Methods for more details), which should not be modified by $H_2{}^{35}S$ (bottom). A significant difference between WT and C53S emerges only when samples are resolved under nonreducing conditions. Mean of ≥3 experiments ± SEM. *$P < 0.05$. (**C**) Scheme of the stepwise chemical reactions leading to persulfidation. (**D**) Quantification of the H_2O_2 uptake performed 2.5 min after addition of 50 μM exogenous H_2O_2 to HyPerCyto-HeLa cells, treated with or without 10 μM DPI for 2.5 hours before and during incubation (30 min) with H_2S. Data were normalized relative to untreated samples. Mean of ≥3 experiments ± SEM.

feature makes sulfenic acid the most plausible oxidative modification that could precede persulfidation of this residue. Therefore, inhibitors of ROS-producing enzymes, like diphenyleneiodonium (DPI), should hinder the H_2S-mediated channel closure by preventing the oxidative modification required for H_2S to react with C53 (see scheme in Fig. 3C). Accordingly, the presence of DPI eliminated transport inhibition (Fig. 3D), consistent with a two-step reaction in which C53 sulfenylation precedes persulfidation (Fig. 3C).

Molecular modeling suggests a mechanism for AQP8 gating

So far, no crystallographic structures are available for AQP8. To further characterize the mechanism of gating, we performed molecular modeling. Taking advantage of the high level of sequence (Fig. 4A and fig. S3) and structural conservation among members of the AQP family (*38*), we built a model of AQP8 using as template the structure of human AQP5 [hAQP5; Protein Data Bank (PDB) code = 3D9S] (*39*), which among all the x-ray structures of human AQPs, shares the highest sequence identity (33%) and coverage (89%) with AQP8. As shown in fig. S4, our model fits precisely in the standards of quality.

The structure emerging from our model is well suited to transport H_2O_2. AQPs contain two asparagine-proline-alanine (NPA) motifs located in the center of the channel that prevent proton translocation (*40*). A second filter is located at the ar/R (aromatic/arginine) constriction site, placed toward the extracellular entrance (Fig. 4, B and C, see light blue area across the two panels), whose dimensions and hydrophobicity determine the selectivity of the different AQPs toward specific solutes (for example, H_2O_2, glycerol, or urea) (*40*). Thus, while in water-selective AQP1 the ar/R constriction site is narrow and polar, it is bigger and more hydrophobic in the *Escherichia coli* glycerol transporter GlpF (fig. S5, left and right panels). Considering the similarities between water and

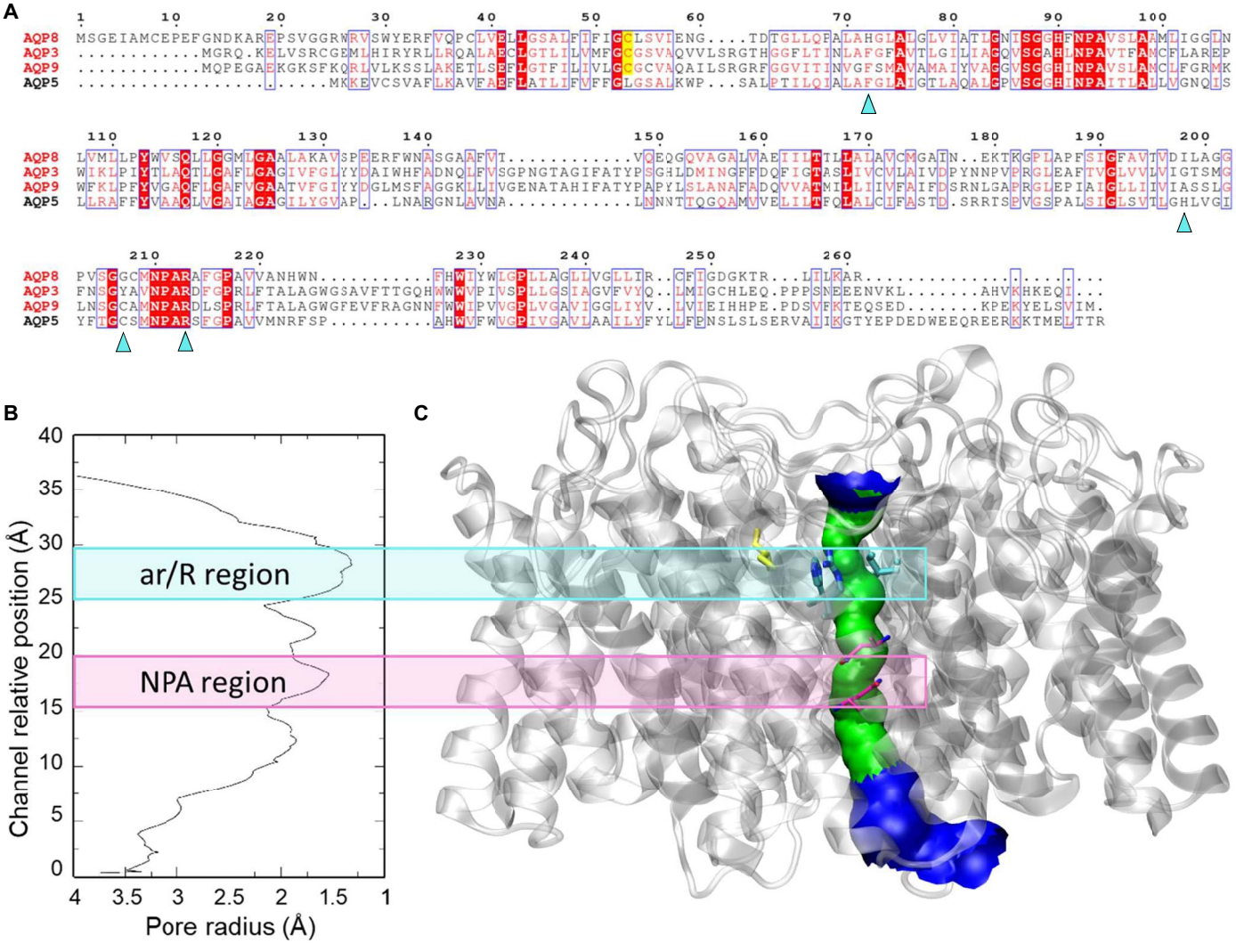

Fig. 4. Molecular modeling of AQP8. (**A**) Sequence alignment of hAQP8 and two other H_2O_2-transporting AQPs (AQP3 and AQP9) with AQP5 (template for homology modeling). Completely conserved residues are highlighted with a red background, highly conserved amino acids colored in red, and highly homologous residues were boxed. The two highly conserved NPA motifs are colored in magenta, the Cys53 is highlighted in yellow, and residues constituting the selectivity filter region (ar/R) are indicated with cyan triangles. (**B** and **C**) Pore profile of AQP8 calculated with HOLE represented as a function of the channel relative position (B) or as multicolored surface (C), illustrating the internal surface of the pore. Green color denotes a pore radius sufficiently large for the passage of a single H_2O_2 molecule. Blue denotes a radius that allows the passage of two H_2O_2 molecules. In (B) and (C), the (ar/R) constriction region and the NPA motif of AQP8 are identified by a cyan and magenta bar, respectively, that goes across both panels. In (C), Cys53 is shown with yellow sticks and the residues forming part of the ar/R or the NPA filters with cyan and magenta sticks.

H_2O_2 molecules, the ar/R constriction region of a peroxiporin is expected to resemble those of water-transporting AQPs. Accordingly, AQP8 and AQP1 constriction sites are composed by the same number and type of amino acids, including the highly conserved R213, the backbone carbonyl of G207, and the side chains of H72 and of I198 (fig. S5, compare left and middle panels). As expected, at the constriction region, the pore of AQP8 is slightly larger as compared to AQP1 with a minimum radius dimension of 1.3 and 0.9 Å, respectively, as calculated by HOLE software (Fig. 4B) (*41*). This is compatible with previous estimates of the minimum radius necessary to accommodate H_2O_2 molecules (*42*) that are ~15% larger than water.

We then analyzed the position and chemical environment of C53. As shown in Fig. 4C, our model predicts that C53 is situated in a restricted region that cannot be reached by any protein. Its side chain points toward the periplasmic space near the ar/R constriction site, so that it ends up partially buried by the highly conserved R213 (Fig. 5A, left panel). Conceivably, the positively charged guanidinium group of R213 reduces the C53 p*K*a value, explaining the high reactivity of this cysteine (*35*). In line with this view, cells expressing a R213A mutant AQP8 were resistant to stress-induced gating (Fig. 5B). To offer a structural explanation of the effects induced by C53 persulfidation on H_2O_2 transport, we modeled the oxidized C53-SSH form (Fig. 5A, right panel). The side chain of the persulfided cysteine does not occupy the center of the pore, implying an indirect role of C53 in channel gating. Instead, the position of H72, which also forms part of the ar/R constriction site, could be of particular functional relevance. The elongated cysteine side chain could affect H72, preventing H_2O_2 passage. Accordingly, the AQP8 H72A mutant was insensitive to stress (Fig. 5B). In support of the specificity of our analysis, mutation of another aromatic residue in the pore (F48) did not influence the sensitivity of the channel to stress (Fig. 5B). All mutants were expressed on the plasma membrane (fig. S6). Together, our results indicate that C53 persulfidation reversibly gates AQP8.

DISCUSSION

Our study identifies a novel mechanism that targets AQP8 and modulates H_2O_2 membrane transport, providing cells with a powerful means to regulate key signaling pathways (*3*–*5*, *21*, *43*, *44*). As H_2O_2 enters cells through AQP8, C53 is oxidized. Its location at the mouth of the channel puts this residue in pole position to react with incoming oxidants. In all likelihood, sulfenylation is not sufficient to inhibit transport through the channel but primes C53 for persulfidation by H_2S locally produced by CBS. The additional sulfur atom modifies the narrow conducting channel, preventing H_2O_2 transport (Fig. 6). The model is based on the well-established notions that (i) AQP8 transports H_2O_2 (*4*, *6*), (ii) AQP8 is gated during diverse stresses (*21*), (iii) persulfidation requires previous oxidation (*9*, *10*, *37*), and (iv) CBS produces H_2S particularly during stress (*29*, *45*, *46*).

H_2S gates AQP8 also in the absence of stress. The long incubation required for full inhibition indicates that H_2S does not directly modify C53, according to its selective reactivity with oxidized cysteines (*9*, *10*, *37*). It follows that a fraction of C53 could be cyclically oxidized in rapidly dividing cells and becomes persulfided in the presence of H_2S. The membrane-impermeant reducing agent MESNA—which can reach C53 and remove the persulfide moiety without interfering with HyPer—promotes permeability in untreated cells as well, suggesting that the persulfidation-based regulatory mechanism acts also in basal conditions, likely adjusting NOX-dependent H_2O_2 fluxes.

Our molecular modeling places C53 in the vicinity of the ar/R constriction, where incoming H_2O_2 molecules align in route to the cytosol. As they traverse the channel, they may thus sulfenylate C53, whose p*K*a is most likely controlled by R213 (*35*). Accordingly, replacing R213 (Fig. 5B) or inhibiting NOX with DPI prevented AQP8 gating induced by stress (*21*) or H_2S (Fig. 3, C and D). Sulfenylation cannot gate the channel per se, otherwise H_2O_2 would close its own transporter before reaching the cytosol. Therefore, this modification could prime C53 for further reaction with H_2S. As shown for other proteins (*15*), persulfidation may also limit oxidation of C53 to SO_2H or SO_3H species, ensuring reversibility of the AQP8 gating mechanism.

As also observed by others (*47*, *48*), in some of our experiments, H_2S was less efficient at concentrations of ≥200 μM. This might indicate that, in the absence of oxidants that generate terminal SOH moieties, H_2S itself may reduce persulfides in the reaction RSSH + H_2S↔RSH + HSSH.

The small caliber of the AQP8 channel (Fig. 4) may explain the difficulties encountered so far in identifying sulfenylated or persulfided C53 by the available labeling protocols (*21*). To overcome this drawback,

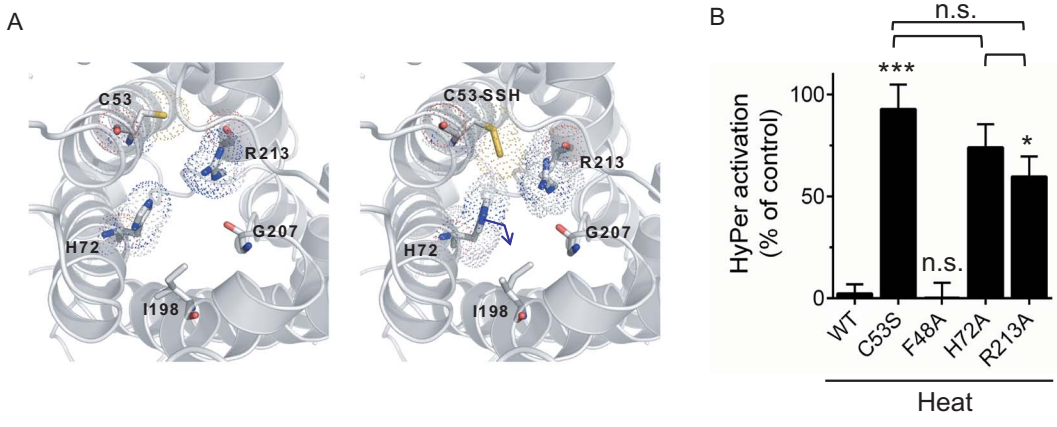

Fig. 5. Role of the amino acids surrounding the constriction site in AQP8 gating. (**A**) The (ar/R) constriction site of AQP8 before (left) or after (right) persulfidation are shown. Protein and residues determining the selectivity filter are represented in cartoon and sticks, respectively. C53, R213, and H72 are highlighted using dots representation. (**B**) Quantification of the H_2O_2 uptake performed 2.5 min after addition of 50 μM exogenous H_2O_2 to HyPerCyto-HeLa cells transfected with different mutants and subjected to heat shock. Data were normalized to the uptake of the respective unstressed samples. Mean of ≥3 experiments ± SEM. n.s., not significant.

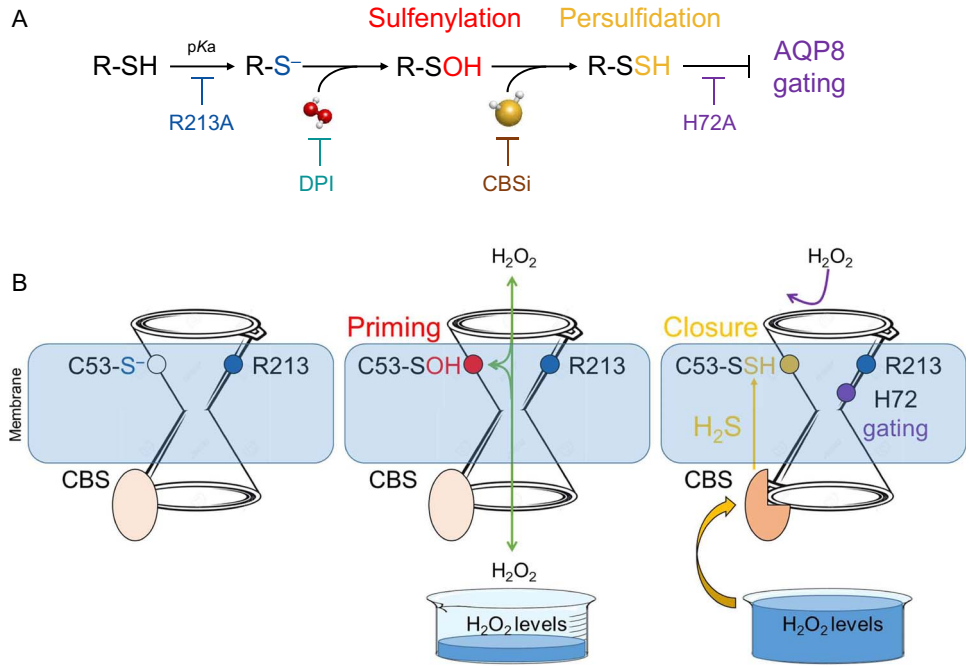

Fig. 6. Two-step inhibition model. (**A**) The scheme summarizes the sequential chemical reactions that lead to AQP8 gating and the ways to inhibit some key steps. (**B**) The left panel depicts AQP8 at steady state, in which C53 is maintained as a thiolate by the positive charge of R213. When H_2O_2 flows through the channel (middle), C53 is sulfenylated, becoming susceptible for further modification by H_2S. When excess H_2O_2 accumulates, like for instance in stressed cells, CBS is activated to produce H_2S inducing, persulfidation of oxidized C53 (right). Elongation of the C53 side chain alters the conformation of the (ar/R) constriction site, presumably leading the aromatic ring of H72 to gate AQP8.

we developed a complex but rewarding strategy aimed at producing radioactive $H_2{}^{35}S$ that subsequently generates -$S^{35}SH$ moieties in sensitive cysteines (Fig. 3A). After extensive controls and normalizations, we were able to consistently detect persulfidation of C53 in AQP8 (Fig. 3B).

Our silencing experiments indicate that CBS is the main source of H_2S that modifies primed C53-SOH. Addition of H_2S restored AQP8 gating in CBS-silenced cells, confirming that production of H_2S by this multifunctional enzyme is required to gate AQP8. It has been proposed that CBS is proteolytically activated during cell stress (*29*, *31*, *46*). The appearance of a CBS-cleaved band in heat-stressed HeLa cells is, thus, in line with our model. The proximity of CBS and AQP8, underscored by the partial co-precipitation of the two proteins, is likely important for the regulatory mechanism. When a threshold is reached, CBS is activated to produce H_2S, which in turn gates AQP8 and limits further H_2O_2 fluxes.

Molecular modeling suggests that persulfidation of C53 indirectly affects the gating mechanism in several possible ways, including steric hindrance with the aromatic ring of H72, or interruption of the hydrogen bonds established by this histidine with H_2O_2 that allow its transport through the pore. The similar phenotype of R213A, C53S, and H72A is in line with the mechanism we propose, as well as with the observation that in the absence of the vicinal positive charge of R213, C53 sulfenylation (and hence persulfidation) is less efficient.

Both C53 and R213 of AQP8 are highly conserved in all the AQP isoforms able to transport H_2O_2 (that is, AQP3 and AQP9) [from the study of Medraño-Fernandez *et al.* (*21*) and fig. S4]. By contrast, H72 is replaced by a phenylalanine, which shows similar bulky hydrophobic properties (fig. S4). This conservation pattern suggests that a similar mechanism of gating could be operating in all the H_2O_2-transporting AQPs, and persulfidation of a highly reactive cysteine might result in channel closure.

How AQP8 permeability is restored remains an open question. Its narrow pore restricts the access to C53 to small, uncharged molecules, virtually excluding proteins even the smallest such as glutathione. Further studies are needed to identify the molecular players involved in channel reopening.

In conclusion, our findings highlight yet another mechanism through which cells integrate diverse signaling pathways to efficiently adapt to environmental changes. Although adaptation is in general beneficial for the host, this mechanism may be detrimental in pathologies such as cancer and chronic inflammation. Thus, H_2S and H_2O_2 generating and conducting systems could represent new therapeutic targets for these disorders.

MATERIALS AND METHODS

Cell culture

HeLa cells were cultured in Dulbecco's modified Eagle's medium (DMEM) + Glutamax-I medium (Life Technologies) supplemented with 10% fetal bovine serum (FBS; EuroClone) and penicillin-streptomycin (5 mg/ml) (Lonza).

Plasmids, small interfering RNAs, and transfection procedures

The plasmid for expression of the HyPer probe targeted to the cytosol (HyPerCyto) was a gift from V. Belousov [Institute of Bioorganic Chemistry (IBCh), Moscow, Russian Federation], whereas silencing-resistant HaloAQP8 WT and C53S plasmids were generated as previously described (*4*). The myc–flag-tagged HaloAQP8 (HaloAQP8mycFlag) was generated into two steps: First, the AQP8 insert was cut from an AQP8–green fluorescent protein (GFP)–expressing plasmid from OriGene (RG219668) and inserted in a vector containing a myc and a Flag tag in tandem (OriGene, RC208083); second, we excided the resulting

AQP8mycFlag fragment and inserted it in the pHTN-Halo plasmid (Promega). Site-directed mutagenesis was carried out with specific primers (*21*) to generate the triple-tagged C53 mutant.

The silencing-resistant Halo-AQP8 R213A, H72A, and F48A plasmids were generated by site-directed mutagenesis using the following primers: HaloAQP8 R213A, 5′-CATGAATCCCGCCGCTGCTTTTG-GAC-3′ (forward) and 5′-GTCCAAAAGCAGCGGCGGGATT-CATG-3′ (reverse); HaloAQP8 H72A, 5′- CTGGCCGCCGGGCTG-GCTTTG-3′ (forward) and 5′-CAAAGCCAGCCCGGCGGCCAG-3′ (reverse); and HaloAQP8 H48A, 5′-TCTGCTCTCGCCATCTT-CATCGGG-3′ (forward) and 5′-CCCGATGAAGATGGCGAGAG-CAGA-3′ (reverse).

The CBS-specific small interfering RNA (siRNA) oligonucleotide (5′-CTCACATCCTAGACCAGTA-3′) and an unrelated control (Block-it) were purchased from Ambion (Life Technologies), and its efficiency was monitored by Western blotting (fig. S2A). For silencing experiments, 8×10^4 HyperCyto-expressing HeLa stable transfectants (see below) were grown overnight in six-well plates and transfected with 30 pmol of siRNA, using RNAiMAX lipofectamin (Invitrogen) according to the manufacturer's instructions. Cells were used after 48 hours. To transiently overexpress WT or mutant HaloAQP8, we transfected cells with JET-PEI (Polyplus-transfection), following the protocol provided by the manufacturer, and cultured them for 48 hours before imaging or biochemical analyses.

Reagents and treatments

NaSH was purchased from Sigma and prepared freshly for each experiment. Briefly, a starting solution of NaHS powder dissolved in distilled water was prepared and then diluted 5000 times and incubated with DNTB [1 mM 5,5′-dithio-bis(2-nitrobenzoic acid)] (Sigma-Aldrich) for 1 to 2 min, yielding a colored product. H_2S concentration was determined by reading the absorbance of this product with a spectrophotometer set at 412 nm using the formula

$$[H_2S] = \text{cuvette volume} * \text{dilution} * OD_{412nm}$$

Working solutions were prepared in Ringer buffer [140 mM NaCl, 2 mM $CaCl_2$, 1 mM $MgSO_4$, 1.5 mM K_2HPO_4, and 10 mM glucose (pH 7.4)]. Cells were washed twice with phosphate-buffered saline (PBS) to remove all FBS to avoid quenching, incubated with different concentrations of NaHS for 30 min at room temperature, and washed twice before confocal analyses. In most experiments, the final concentration was 100 or 500 μM for untransfected or AQP8-overexpressing cells, respectively.

Extracellular catalase (CAT, 5000 U/ml in Ringer buffer), DPI (10 μM in DMEM for 3 hours), DTT (5 mM in Ringer buffer), H_2O_2 (50 μM in Ringer buffer), MESNA (10 mM in Ringer buffer), tangeretin (200 μM in complete medium), and CHX (0.5 mM, see below) were all purchased from Sigma-Aldrich. Heat shock was performed as described (*21*).

Imaging HyPer oxidation

To perform confocal live imaging experiments, 8×10^4 HyperCyto-expressing HeLa cells were silenced and/or transfected on glass coverslips as described above. To identify HaloAQP8-expressing cells, we added 2 nM HaloTag tetramethylrhodamine (TMR) Direct Ligand (Promega) 24 hours after transfection. After 24 hours of culture with the fluorescent ligand, cells on coverslips were equilibrated in Ringer buffer for 10 min at room temperature before addition of freshly prepared H_2O_2.

Confocal images were collected every 2 s for 5 min or more by dual excitation with a 488-nm argon and a 405-nm violet diode lasers. We used an ultraview confocal laser scanning microscope equipped with a 40× oil-immersion lens (PerkinElmer). The 488/405-nm ratios were calculated by ImageJ software for ≥25 cells, averaged, and showed as mean fold change ratio plotted against time ± SEM. To facilitate quantification and statistical analyses, in some experiments, we averaged the data obtained in the time course experiments performed after 2.5 min after H_2O_2 addition and represented them as the percentage of H_2O_2 transport in H_2S-treated cells relative to the corresponding untreated cells. At least three independent experiments were performed for each condition.

Antibodies and Western blotting

Rabbit anti-CBS was purchased from Merck-Millipore. Rabbit anti-Halo was obtained from Promega. Mouse anti-tubulin and rabbit anti-calnexin were from Sigma. Secondary antibodies anti-mouse and anti-rabbit Alexa Fluor 488 or Alexa Fluor 647 were purchased from Invitrogen. Images were acquired using a Typhoon FLA-9000 (GE HealthCare), processed with ImageJ and densitometrically quantified when indicated by ImageJ ±SEM.

Co-immunoprecipitation

HeLa cells transiently expressing either the Halo protein alone or the recombinant proteins HaloAQP8mycFlag or calnexin-Flag were lysed in radioimmunoprecipitation assay (RIPA) buffer [0.1% SDS, 1% NP40, 150 mM NaCl, 50 mM tris (pH 7.4)] supplemented with 10 mM *N*-ethylmaleimide (NEM, Sigma) and protease and phosphatase inhibitor cocktails (Roche). Post-nuclear cell lysates were immunoprecipitated using anti-flag M2 affinity gel (Sigma), following standard procedures. Immune-complexes and total lysates were resolved by SDS-polyacrylamide gels, transferred to nitrocellulose membranes, and immunoblotted with the indicated antibodies.

Radioactive tracing of persulfidation

Cells transfected with WT or C53S HaloAQP8mycFlag were seeded in 6-cm plates at 2.5×10^6 cells per plate and incubated overnight in the presence of 30 nM HaloTag TMR Direct Ligand. Cells were preincubated for 30 min in methionine/cysteine-free DMEM supplemented with 1% dialyzed FBS at 37°C, followed by further 60 min in the same conditions but in the presence of 0.5 mM CHX. Cells were then labeled for 3 hours with [^{35}S]cys/met (0.22 mCi/ml) (EasyTag, PerkinElmer) at 37° or 42°C, in the continuous presence of 0.5 mM CHX. Cells were then washed in ice-cold PBS and lysed in RIPA buffer containing 1 mM NEM, protease, and phosphatase inhibitors. The anti-flag M2 immunoprecipitates were resolved by SDS–polyacrylamide gel electrophoresis and blotted. Signals from TMR-direct Halo ligand, which label all AQP8 present at the start of the radioactive labeling, were acquired with a Typhoon FLA-9000 and acted as convenient loading control. Under these conditions, we expect part of the radioactive sulfur to be converted into H_2S by the transsulfuration pathway. To account for the residual protein synthesis during prolonged labeling, we reduced aliquots from the samples by 200 mM DTT before electrophoresis to selectively eliminate persulfided moieties. The difference between the signal in nonreduced and reduced conditions represents the extent of persulfidation that has occurred in the 3-hour labeling.

Radioactive signal was quantified using ImageJ and normalized using the signal from the Halo ligand [*Persulfidation index*(PI) $= \frac{^{35}S}{\text{Halo ligand}}$]. As reference, we choose to use the C53S mutant because it lacks the residue target of the inhibition, and PI was represented as fold increase for each condition (Fold increase of $PI_{yx} = \frac{PI_{yx}}{PI_{C53Sx}}$, where y is the AQP8 form and x is the condition under consideration) ±SEM. An average of four experiments is shown.

Molecular modeling of hAQP8 and of its persulfided form

The three-dimensional (3D) model of hAQP8 was generated using as template the crystallographic structure of hAQP5 (3D9S; resolution = 2 Å) (*39*). The tetramer was built using swiss-model web server (*49*) and validated through the ProSA web interface (*50*), where the global quality of each chain was assessed through the z score (−5.73, −5.62, −5.69, and −5.58) (fig. S5B). The model was then refined exploiting the Protein Preparation Wizard, available in Maestro Software Package (*51*): Hydrogens were added; the orientation of the hydroxyl groups of Ser, Thr, and Tyr and the side chains of Asn and Gln residues were optimized; the protonation states were chosen according to the experimental pH; and a minimization using an OPLS 2005 force field (*52*) with a root mean square deviation tolerance on heavy atom of 0.3 Å was performed. Starting from the AQP8 model, we generated its persulfided form, converting the C53 side chain in C53-SSH with Maestro Software (*51*). The AQP8 C53-SSH was finally minimized (*52*).

Characterizing the channel

The package HOLE (*41*) was used to evaluate the pore diameter for the hAQP8 model. Within this package, using Assisted model building with Energy refinement (AMBER) values for van der Waals atomic radii, the minimum pore radius of 1.3 Å was recovered at the selectivity region (ar/R) compatible with the minimum radius necessary to accommodate a hydrogen peroxide molecule (~15% larger than that of water, with r_{water} = 1.15 Å) as proposed by Smart *et al.* (*41*) and Almasalmeh *et al.* (*42*). A radius of 1.3 Å is the minimum required for a H_2O_2 molecule showing that this form of AQP8 would be filled with H_2O_2 molecules under normal conditions.

Alignments

Alignment was performed with Clustal X v2.0 (*53*) and represented with ESPript3.0 (*54*).

Statistical analyses

The two-sample t test was used for independent samples or the one-way analysis of variance (ANOVA) method for multiple samples. When using the latter, the Tukey honest significant difference post hoc test was also applied to find out which groups were significantly different from which others. In all cases, statistical significance was defined as $^*P < 0.05$, $^{**}P < 0.01$, or $^{***}P < 0.001$.

SUPPLEMENTARY MATERIALS

Supplementary material for this article is available at http://advances.sciencemag.org/cgi/content/full/4/5/eaar5770/DC1

fig. S1. H_2S treatment kinetics and titration.
fig. S2. CBS quantifications and tangeritin effect.
fig. S3. Sequence alignment of all human members of the AQP family.
fig. S4. Analysis of quality of the AQP8 homology model.
fig. S5. ar/R constriction region of AQP1, AQP8, and GlpF.
fig. S6. Subcellular localization of the HaloAQP8 F48A, H72A, and R213A mutants.
movie. S1. H_2O_2 uptake of AQP8 WT-expressing cells treated with H_2S.
movie. S2. H_2O_2 uptake of AQP8 C53S-expressing cells treated with H_2S.

REFERENCES AND NOTES

1. H. Sies, C. Berndt, D. P. Jones, Oxidative stress. *Annu. Rev. Biochem.* **86**, 715–748 (2017).
2. B. D. Paul, S. H. Snyder, H2S: A novel gasotransmitter that signals by sulfhydration. *Trends Biochem. Sci.* **40**, 687–700 (2015).
3. E. W. Miller, B. C. Dickinson, C. J. Chang, Aquaporin-3 mediates hydrogen peroxide uptake to regulate downstream intracellular signaling. *Proc. Natl. Acad. Sci. U.S.A.* **107**, 15681–15686 (2010).
4. M. Bertolotti, S. Bestetti, J. M. García-Manteiga, I. Medraño-Fernandez, A. Dal Mas, M. L. Malosio, R. Sitia, Tyrosine kinase signal modulation: A matter of H_2O_2 membrane permeability? *Antioxid. Redox Signal.* **19**, 1447–1451 (2013).
5. S. Watanabe, C. S. Moniaga, S. Nielsen, M. Hara-Chikuma, Aquaporin-9 facilitates membrane transport of hydrogen peroxide in mammalian cells. *Biochem. Biophys. Res. Commun.* **471**, 191–197 (2016).
6. G. P. Bienert, J. K. Schjoerring, T. P. Jahn, Membrane transport of hydrogen peroxide. *Biochim. Biophys. Acta* **1758**, 994–1003 (2006).
7. O. Kabil, R. Banerjee, Redox biochemistry of hydrogen sulfide. *J. Biol. Chem.* **285**, 21903–21907 (2010).
8. R. Banerjee, Catalytic promiscuity and heme-dependent redox regulation of H_2S synthesis. *Curr. Opin. Chem. Biol.* **37**, 115–121 (2017).
9. D. Zhang, I Macinkovic, N. O. Devarie-Baez, J. Pan, C.-M. Park, K. S. Carroll, M. R. Filipovic, M. Xian, Detection of protein S-sulfhydration by a tag-switch technique. *Angew. Chem. Int. Ed. Engl.* **53**, 575–581 (2014).
10. E. Cuevasanta, M. Lange, J. Bonanata, E. L. Coitiño, G. Ferrer-Sueta, M. R. Filipovic, B. Alvarez, Reaction of Hydrogen Sulfide with Disulfide and Sulfenic Acid to Form the Strongly Nucleophilic Persulfide. *J. Biol. Chem.* **290**, 26866–26880 (2015).
11. M. Nishida, T. Sawa, N. Kitajima, K. Ono, H. Inoue, H. Ihara, H Motohashi, M. Yamamoto, M. Suematsu, H. Kurose, A van der Vliet, B. A. Freeman, T. Shibata, K. Uchida, Y. Kumagai, T. Akaike, Hydrogen sulfide anion regulates redox signaling via electrophile sulfhydration. *Nat. Chem. Biol.* **8**, 714–724 (2012).
12. G. Yang, K. Zhao, Y. Ju, S. Mani, Q. Cao, S. Puukila, N. Khaper, L. Wu, R. Wang, Hydrogen sulfide protects against cellular senescence *via S*-sulfhydration of Keap1 and activation of Nrf2. *Antioxid. Redox Signal.* **18**, 1906–1919 (2013).
13. Y. Kimura, H. Kimura, Hydrogen sulfide protects neurons from oxidative stress. *FASEB J.* **18**, 1165–1167 (2004).
14. B. Qabazard, L. Li, J. Gruber, M. T. Peh, L. F. Ng, S. D. Kumar, P. Rose, C. H. Tan, B. W. Dymock, F. Wei, S. C. Swain, B. Halliwell, S. R. Stürzenbaum, P. K. Moore, Hydrogen sulfide is an endogenous regulator of aging in Caenorhabditis elegans. *Antioxid. Redox Signal.* **20**, 2621–2630 (2014).
15. M. R. Filipovic, Persulfidation (S-sulfhydration) and H_2S. *Handb. Exp. Pharmacol.* **230**, 29–59 (2015).
16. W. Zhang, C. Xu, G. Yang, L. Wu, R. Wang, Interaction of H_2S with calcium permeable channels and transporters. *Oxid. Med. Cell. Longev.* **2015**, 323269 (2015).
17. B. Olas, Hydrogen sulfide as a "Double-Faced" compound: One with pro- and antioxidant effect. *Adv. Clin. Chem.* **78**, 187–196 (2017).
18. J. C. Mathai, A. Missner, P. Kügler, S. M. Saparov, M. L. Zeidel, J. K. Lee, P. Pohl, No facilitator required for membrane transport of hydrogen sulfide. *Proc. Natl. Acad. Sci. U.S.A.* **106**, 16633–16638 (2009).
19. E. Cuevasanta, M. N. Möller, B. Alvarez, Biological chemistry of hydrogen sulfide and persulfides. *Arch. Biochem. Biophys.* **617**, 9–25 (2017).
20. G. P. Bienert, I. Mendraño-Fernandez, R. Sitia, Regulation of H_2O_2 transport across cell membranes, *in Hydrogen Peroxide Metabolism in Health and Disease*, M. C. M. Vissers, M. Hampton, A. J, Kettle, Ed. (Taylor & Francis Group, 2017).
21. I. Medraño-Fernandez, S. Bestetti, M. Bertolotti, G. P. Bienert, C. Bottino, U. Laforenza, A. Rubartelli, R. Sitia, Stress Regulates Aquaporin-8 Permeability to Impact Cell Growth and Survival. *Antioxid. Redox Signal.* **24**, 1031–1044 (2016).
22. C. X. C Santos, L. Y. Tanaka, J. Wosniak Jr., F. R. M. Laurindo, Mechanisms and implications of reactive oxygen species generation during the unfolded protein response: Roles of endoplasmic reticulum oxidoreductases, mitochondrial electron transport, and NADPH oxidase. *Antioxid. Redox Signal.* **11**, 2409–2427 (2009).
23. F. Jiang, Y. Zhang, G. J. Dusting, NADPH oxidase-mediated redox signaling: Roles in cellular stress response, stress tolerance, and tissue repair. *Pharmacol. Rev.* **63**, 218–242 (2011).
24. W.-J. Kwak, G.-S. Kwon, I. Jin, H. Kuriyama, H.-Y. Sohn, Involvement of oxidative stress in the regulation of H_2S production during ultradian metabolic oscillation of *Saccharomyces cerevisiae*. *FEMS Microbiol. Lett.* **219**, 99–104 (2003).
25. V. Yadav, X. H. Gao, B. Willard, M. Hatzoglou, R. Banerjee, O. Kabil, Hydrogen sulfide modulates eukaryotic translation initiation factor 2α (eIF2α) phosphorylation status in the integrated stress-response pathway. *J. Biol. Chem.* **292**, 13143–13153 (2017).
26. V. V. Belousov, A. F. Fradkov, K. A. Lukyanov, D. B. Staroverov, K. S. Shakhbazov, A. V. Terskikh, S. Lukyanov, Genetically encoded fluorescent indicator for intracellular hydrogen peroxide. *Nat. Methods* **3**, 281–286 (2006).

27. R. J. Reiffenstein, W. C. Hulbert, S. H. Roth, Toxicology of hydrogen sulfide. *Annu. Rev. Pharmacol. Toxicol.* **32**, 109–134 (1992).
28. R. Banerjee, R. Evande, O. Kabil, S. Ojha, S. Taoka, Reaction mechanism and regulation of cystathionine β-synthase. *Biochim. Biophys. Acta* **1647**, 30–35 (2003).
29. R. Banerjee, C. G. Zou, Redox regulation and reaction mechanism of human cystathionine-β-synthase: A PLP-dependent hemesensor protein. *Arch. Biochem. Biophys.* **433**, 144–156 (2005).
30. M. K. Thorson, T. Majtan, J. P. Kraus, A. M. Barrios, Identification of cystathionine β-synthase inhibitors using a hydrogen sulfide selective probe. *Angew. Chem. Int. Ed. Engl.* **52**, 4641–4644 (2013).
31. C.-G. Zou, R. Banerjee, Tumor necrosis factor-α-induced targeted proteolysis of cystathionine β-synthase modulates redox homeostasis. *J. Biol. Chem.* **278**, 16802–16808 (2003).
32. C.-M. Park, I. Macinkovic, M. R. Filipovic, M. Xian, Use of the "tag-switch" method for the detection of protein S-sulfhydration. *Methods Enzymol.* **555**, 39–56 (2015).
33. E. Doka, I. Macinkovic, M. R. Filipovic, M. Xian, A novel persulfide detection method reveals protein persulfide- and polysulfide-reducing functions of thioredoxin and glutathione systems. *Sci. Adv.* **2**, e1500968 (2016).
34. R. Wedmann, C. Onderka, S. Wei, I. A. Szijártó, J. L. Miljkovic, A. Mitrovic, M. Lange, S. Savitsky, P. K. Yadav, R. Torregrossa, E. G. Harrer, T. Harrer, I. Ishii, M. Gollasch, M. E. Wood, E. Galardon, M. Xian, M. Whiteman, R. Banerjee, M. R. Filipovic, Improved tag-switch method reveals that thioredoxin acts as depersulfidase and controls the intracellular levels of protein persulfidation. *Chem. Sci.* **7**, 3414–3426 (2016).
35. M. Lo Conte, K. S. Carroll, The redox biochemistry of protein sulfenylation and sulfinylation. *J. Biol. Chem.* **288**, 26480–26488 (2013).
36. M. H. Stipanuk, Sulfur amino acid metabolism: Pathways for production and removal of homocysteine and cysteine. *Annu. Rev. Nutr.* **24**, 539–577 (2004).
37. T. V. Mishanina, M. Libiad, R. Banerjee, Biogenesis of reactive sulfur species for signaling by hydrogen sulfide oxidation pathways. *Nat. Chem. Biol.* **11**, 457–464 (2015).
38. V. M. Unger, Fraternal twins: AQP1 and GlpF. *Nat. Struct. Biol.* **7**, 1082–1084 (2000).
39. R. Horsefield, K. Nordén, M. Fellert, A. Backmark, S. Törnroth-Horsefield, A. C. Terwisscha van Scheltinga, J. Kvassman, P. Kjellbom, U. Johanson, R. Neutze, High-resolution x-ray structure of human aquaporin 5. *Proc. Natl. Acad. Sci. U.S.A.* **105**, 13327–13332 (2008).
40. J. S. Hub, B. L. de Groot, Mechanism of selectivity in aquaporins and aquaglyceroporins. *Proc. Natl. Acad. Sci. U.S.A.* **105**, 1198–1203 (2008).
41. O. S. Smart, J. M. Goodfellow, B. A. Wallace, The pore dimensions of gramicidin A. *Biophys. J.* **65**, 2455–2460 (1993).
42. A. Almasalmeh, D. Krenc, B. Wu, E. Beitz, Structural determinants of the hydrogen peroxide permeability of aquaporins. *FEBS J.* **281**, 647–656 (2014).
43. M. Hara-Chikuma, S. Watanabe, H. Satooka, Involvement of aquaporin-3 in epidermal growth factor receptor signaling via hydrogen peroxide transport in cancer cells. *Biochem. Biophys. Res. Commun.* **471**, 603–609 (2016).
44. M. Bertolotti, G. Farinelli, M. Galli, A. Aiuti, R. Sitia, AQP8 transports NOX2-generated H_2O_2 across the plasma membrane to promote signaling in B cells. *J. Leukoc. Biol.* **100**, 1071–1079 (2016).
45. S. Taoka, S. Ohja, X. Shan, W. D. Kruger, R. Banerjee, Evidence for heme-mediated redox regulation of human cystathionine β-synthase activity. *J. Biol. Chem.* **273**, 25179–25184 (1998).
46. W.-N. Niu, P. K. Yadav, J. Adamec, R. Banerjee, S-glutathionylation enhances human cystathionine β-synthase activity under oxidative stress conditions. *Antioxid. Redox Signal.* **22**, 350–361 (2015).
47. C. Szabo, C. Ransy, K. Módis, M. Andriamihaja, B. Murghes, C. Coletta, G. Olah, K. Yanagi, F. Bouillaud, Regulation of mitochondrial bioenergetic function by hydrogen sulfide. Part I. Biochemical and physiological mechanisms. *British journal of pharmacology* **171**, 2099–2122 (2014).
48. J. R. Koenitzer, T. S. Isbell, H. D. Patel, G. A. Benavides, D. A. Dickinson, R. P. Patel, V. M. Darley-Usmar, J. R. Lancaster Jr., J. E. Doeller, D. W. Kraus, Hydrogen sulfide mediates vasoactivity in an O_2-dependent manner. *Am. J. Physiol. Heart Circ. Physiol.* **292**, H1953–H1960 (2007).
49. M. Biasini, S. Bienert, A. Waterhouse, K. Arnold, G. Studer, T. Schmidt, F. Kiefer, T. Gallo Cassarino, M. Bertoni, L. Bordoli, T. Schwede, SWISS-MODEL: Modelling protein tertiary and quaternary structure using evolutionary information. *Nucleic Acids Res.* **42**, W252–W258 (2014).
50. M. Wiederstein, M. J. Sippl, ProSA-web: Interactive web service for the recognition of errors in three-dimensional structures of proteins. *Nucleic Acids Res.* **35**, W407–W410 (2007).
51. G. M. Sastry, M. Adzhigirey, T. Day, R. Annabhimoju, W. Sherman, Protein and ligand preparation: Parameters, protocols, and influence on virtual screening enrichments. *J. Comput. Aided Mol. Des.* **27**, 221–234 (2013).
52. G. A. Kaminski, R. A. Friesner, J. Tirado-Rives, W. L. Jorgensen, Evaluation and reparametrization of the OPLS-AA force field for proteins via comparison with accurate quantum chemical calculations on peptides. *J. Phys. Chem. B* **105**, 6474–6487 (2001).
53. M. A. Larkin, G. Blackshields, N. P. Brown, R Chenna, P. A. McGettigan, H. McWilliam, F. Valentin, I. M. Wallace, A. Wilm, R. Lopez, J. D. Thompson, T. J. Gibson, D. G. Higgins, Clustal W and Clustal X version 2.0. *Bioinformatics* **23**, 2947–2948 (2007).
54. X. Robert, P. Gouet, Deciphering key features in protein structures with the new ENDscript server. *Nucleic Acids Res.* **42**, W320–W324 (2014).

Acknowledgments: We thank all members of our laboratory, P. Panina, L. Rampoldi, and E. van Anken (San Raffaele Scientific Institute, Milan, Italy); E. Doká and P. Nagy (National Institute of Oncology, Budapest, Hungary); and E. Avezov (Cambridge University, UK) for useful suggestions and constructive criticisms. Because of space limitations, as well as restriction of cited references, we apologize to all those colleagues and researchers in the field whose work is not directly cited here. **Funding:** This work was supported in part through grants from the Associazione Italiana Ricerca sul Cancro (IG 2016-18824 to R.S. and IG 2016-15434 to A.R.), the Fondazione Cariplo (2015-0591 to R.S.), the Ministero della Salute (PE-2011-02352286 to R.S. and RF-2013-02354880 to G.M.), the Telethon (GGP15059 to R.S.), and the "Cinque per mille" (to A.R.). G.P.B. was supported by an Emmy Noether grant 1668/1-1 from the Deutsche Forschungsgemeinschaft. **Author contributions:** S.B., I.M.-F., A.R., and R.S. designed the strategy of the study. S.B. performed the imaging experiments. I.M.-F. performed the biochemical assays. M. Galli prepared cells and transfections. M. Ghitti and G.M. generated and analyzed the 3D model of AQP8. A.O. performed the radioactive labeling. All authors contributed in interpreting the data. S.B., I.M.-F., M. Ghitti, and R.S. wrote the manuscript. **Competing interest:** The authors declare that they have no competing interests. **Data and materials availability:** All data needed to evaluate the conclusions in the paper are present in the paper and/or the Supplementary Materials. Additional data related to this paper may be requested from the authors.

Submitted 23 November 2017
Accepted 16 March 2018
Published 2 May 2018
10.1126/sciadv.aar5770

Citation: S. Bestetti, I. Medraño-Fernandez, M. Galli, M. Ghitti, G. P. Bienert, G. Musco, A. Orsi, A. Rubartelli, R. Sitia, A persulfidation-based mechanism controls aquaporin-8 conductance. *Sci. Adv.* **4**, eaar5770 (2018).